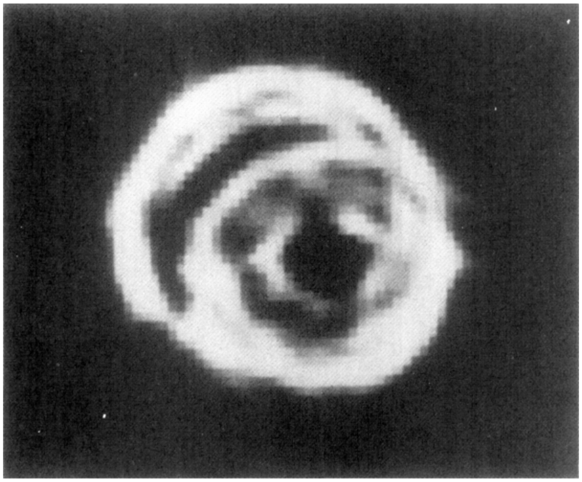

Fig. 4.34: *An attenuation reconstruction obtained by using the frequency-shift method. (From [Kak79].)*

grams. In addition, the design of a program to automatically diagnose breast tomograms based on the attenuation constant and the index of refraction near the lesion was described.

The mammograms and ultrasound tomographic images in Figs. 4.35 and 4.36, respectively, show a small spiculated cancer in the upper outer quadrant of a right breast. The tomographic reconstructions shown in Fig. 4.36 were based on the measurement of 60 parallel projections each with 200 rays. For each ray the time of arrival and the signal level of a 5-MHz ultrasound signal were measured and stored on tape for off-line processing. The total data collection time was 5 minutes.

In this study the attenuation and refractive index images were based on a full wave rectified and low pass filtered version of the measured ultrasonic pressure wave. The time delay caused by the object was measured by timing the instant when the filtered signal first crossed a threshold. This gives a direct estimate of the time delay, T_d, as described in Section 4.3.2. On the other hand, the attenuation of the signal was measured by integrating the first two microseconds of the filtered signal. While this method doesn't take into account the frequency dependence of the attenuation coefficient, it does have the overriding advantage that its hardware implementation is very simple and fast.

4.4 Magnetic Resonance Imaging[7]

No book describing tomographic imaging would be complete without a discussion of (nuclear) magnetic resonance imaging (MRI). While the principles of nuclear magnetic resonance have been well known since the

[7] We appreciate the help of Kevin King of General Electric's Medical Systems Group and Greg Kirk of Resonex, Inc. in preparing this material.

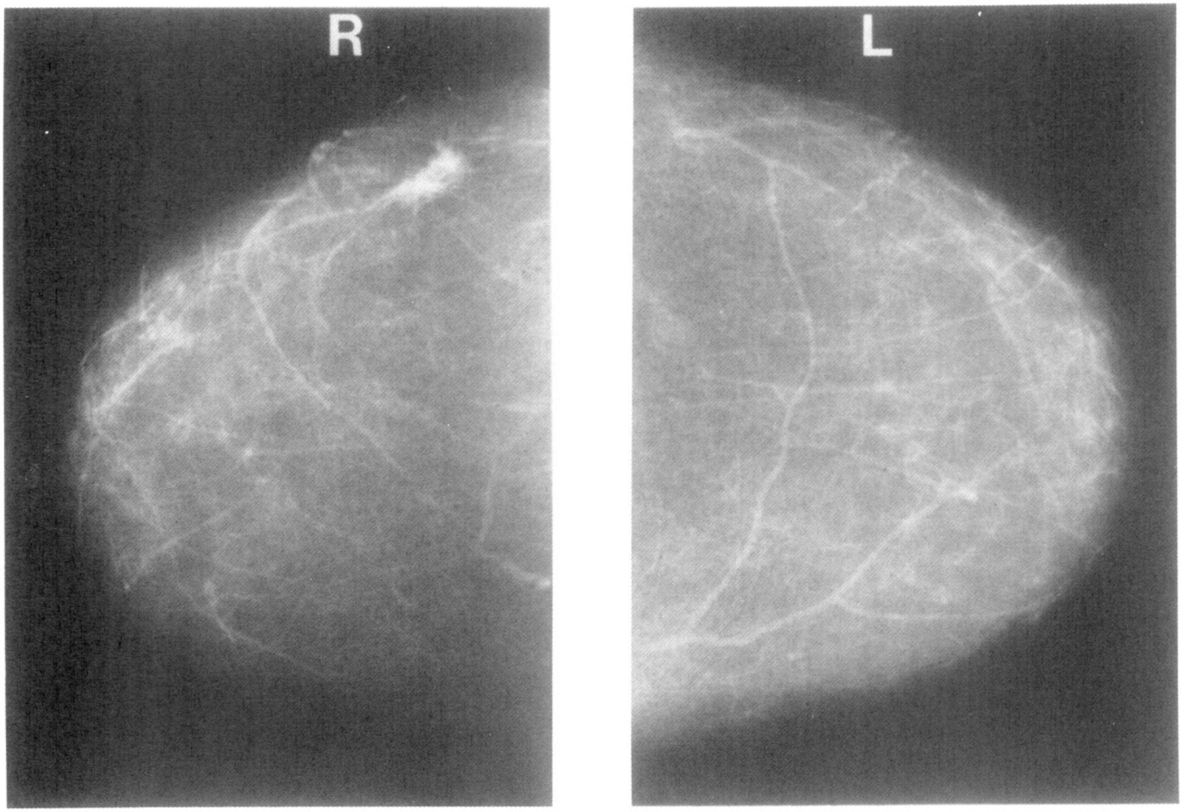

Fig. 4.35: *The x-ray mammograms of these female breasts show a small spiculated cancer in the upper outer quadrant of the right breast. (Courtesy of Jim Greenleaf of the Mayo Clinic in Rochester, MN.)*

1950s, only since 1972 has it been used for imaging. In the sense that the images produced represent a cross section of the object, MRI is a tomographic technique. Two head images obtained using MRI are shown in Fig. 4.37.

The fundamentals of chemistry and physics required to derive MRI are beyond the scope of this book. A rigorous derivation requires the use of quantum mechanics, but since acceptable models of the process can be built using classical mechanics, this will be the approach used here. For more information the reader is referred to excellent accounts of the theory in [Man82], [Mac83], [Cho82], [Hin83], [Pyk82].

Magnetic resonance imaging is based on the measurement of radio frequency electromagnetic waves as a spinning nucleus returns to its equilibrium state. Any nucleus with an odd number of particles (protons and neutrons) has a magnetic moment, and, when the atom is placed in a strong magnetic field, the moment of the nucleus tends to line up with the field. If the atom is then excited by another magnetic field it emits a radio frequency signal as the nucleus returns to its equilibrium position. Since the frequency of the signal is dependent on not only the type of atom but also the magnetic

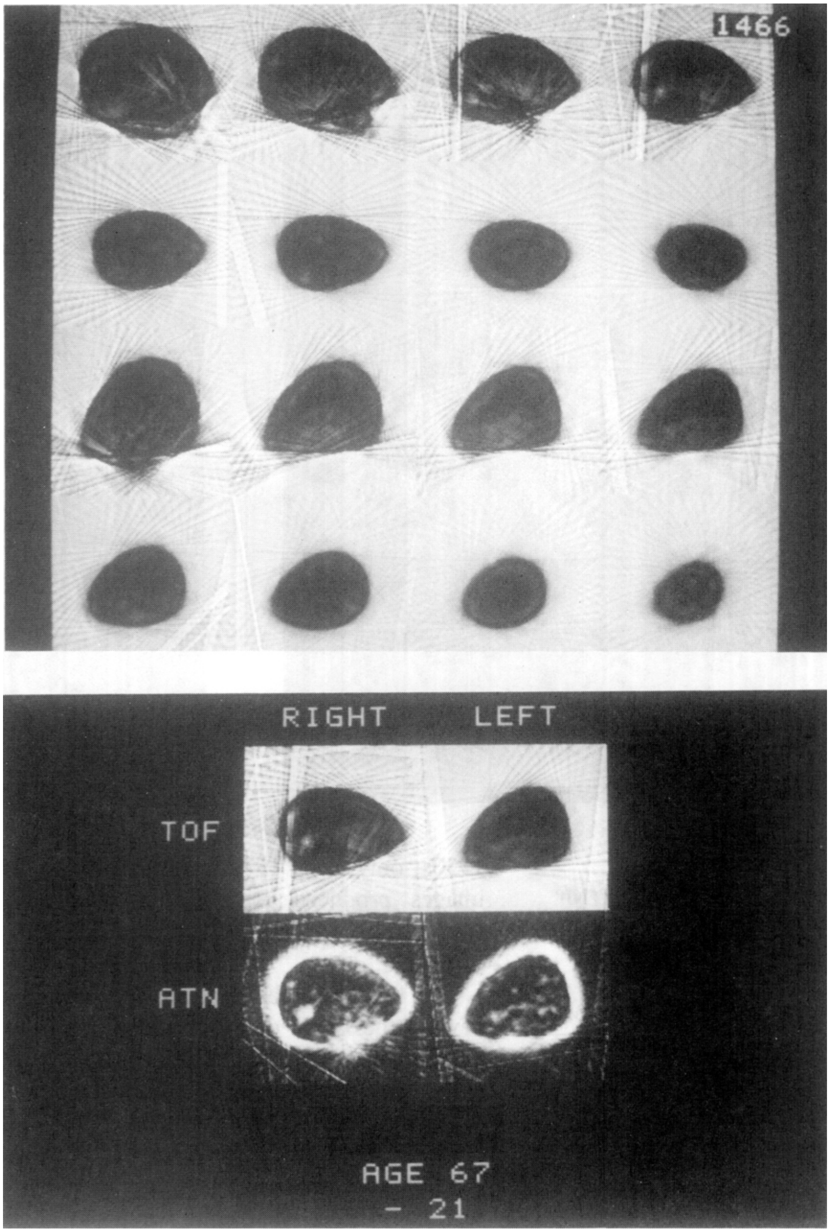

Fig. 4.36: *The time of flight (TOF) images on top and the combined TOF and attenuation (ATN) images on the bottom show the small cancer. (Reprinted with permission from [Sch84].)*

fields present, the position and type of each nucleus can be detected by appropriate signal processing.

Two of the more interesting atoms for MRI are hydrogen and phosphorus. The hydrogen atom is found most often bound into a water molecule while phosphorus is an important link in the transfer of energy in biological

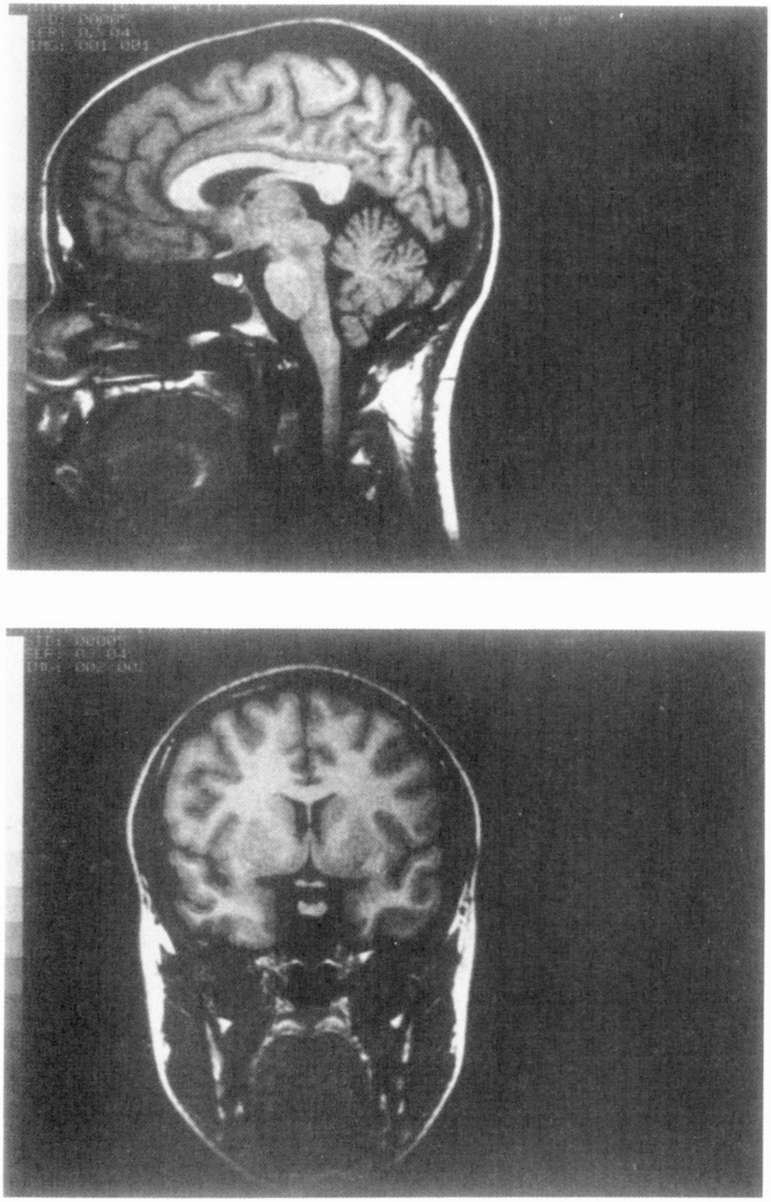

Fig. 4.37: *These two images demonstrate the contrast and resolution obtainable using MRI. They were obtained using a 1.5-Tesla Signa® system at General Electric's MR Development Center. (Courtesy of General Electric's Medical Systems Group.)*

systems. Both of these atoms have an odd number of nucleons and thus act like a spinning magnetic dipole when placed into a strong field.

When a spinning magnetic moment is placed in a strong magnetic field and perturbed it precesses much like a spinning top or gyroscope. The frequency of precession is determined by the magnitude of the external field and the type and chemical binding of the atom. The precession frequency is known as the

Larmor frequency and is given by

$$\omega = \gamma H \tag{59}$$

where H is the magnitude of the local magnetic field and γ is known as the gyromagnetic constant. The gyromagnetic constant, although primarily a function of the type of nucleus, also changes slightly due to the chemical elements surrounding the nucleus. These small changes in the gyromagnetic constant are known as chemical shifts and are used in NMR spectroscopy to identify the compounds in a sample. In MRI, on the other hand, a spatially varying field is used to code each position with a unique resonating frequency. Image reconstruction is done using this information.

Recalling that a magnetic field has both a magnitude and direction at a point in three space, (x, y, z), the field is described by the vector quantity $\vec{H}(x, y, z)$. When necessary we will use the orthogonal unit vectors $\hat{x}$, $\hat{y}$, and $\hat{z}$ to represent the three axes. Conventionally, the z-axis is aligned along the axis of the static magnetic field used to align the magnetic moments. The static magnetic field is then described by $\vec{H}_0 = H_0\hat{z}$.

A radio frequency magnetic wave in the (x, y)-plane and at the Larmor frequency, $\omega_0 = \gamma H_0$, is used to perturb the magnetic moments from their equilibrium position. The degree of tipping or precession that occurs is dependent on the strength of the field and the length of the pulse. Using the classical mechanics model a sinusoidal field of magnitude H_1 that lasts t_p seconds will cause the magnetic moment to precess through an angle given by

$$\theta = \gamma H_1 t_p. \tag{60}$$

The actual transmitted field, $\vec{H}_1(x, y, z)$, is given by

$$\vec{H}_1(x, y, z) = 2H_1 \cos \omega_0 t \, \hat{x}. \tag{61}$$

Generally, H_1 and t_p are varied so that the moment will be flipped either 90 or 180°. By flipping the moments 90° the maximum signal is obtained as the system returns to equilibrium while 180° flips are often used to change the sign of the phase (with respect to the $H_{\hat{1}}$-axis) of the moment.

It is important to note that only those nuclei where the magnitude of the local field is H_0 will flip according to (60). Those nuclei with a local magnetic field near H_0 will flip to a small degree while those nuclei with a local field far from H_0 will not be flipped at all. This property of spinning nuclei in a magnetic field is used in MRI to restrict the active nuclei to restricted sections of the body [Man82]. Typical slice thicknesses in 1986 machines are from 3 to 10 mm.

After the radio frequency (RF) pulse is applied there are two effects that can be measured as the magnetic moment returns to its equilibrium position. They are known as the longitudinal and transverse relaxation times. The longitudinal or spin-lattice relaxation time, T_1, is the simpler of the two and represents the time it takes for the energy to dissipate and the moment to return to its equilibrium position along the $\hat{z}$-axis. In addition, after the RF pulse is applied, the spinning magnetic moments gradually become out of phase due to the effects of nearby nuclei. The time for this to occur is known as the transverse or spin-spin relaxation time, T_2. In practice, there is a third parameter called T_2^* that also takes into account the local inhomogeneities of the magnetic field. Because of physical constraints the following relationship always holds:

$$T_2^* \leq T_2 \leq T_1. \tag{62}$$

Note that T_2^* includes the effect of T_2.

The process of tipping (or even flipping) a moment and its eventual return to the equilibrium state are diagrammed in Fig. 4.38. Conventionally the magnetic moments are shown in a coordinate system that rotates at the Larmor frequency. The direction of the magnetic moment before and immediately after a 45° pulse is shown in Figs. 4.38(a) and (b). Fig. 4.38(c) diagrams the moments as they start to return to the equilibrium position and some of the moments become out of phase. The time T_2 is shorter than T_1 so the moments are totally out of phase before they return to the equilibrium position. This is shown in Fig. 4.38(d). Finally, after several T_1 intervals the moments return to their equilibrium position as shown in Fig. 4.38(e).

As the spinning moments return to their equilibrium position they generate an electromagnetic wave at the Larmor frequency. This wave is known as the free induction decay (FID) signal and can be detected using coils around the object. When the magnetic moments are in phase, as they are immediately following an RF excitation, the FID signal is proportional to both the density and the transverse component of the magnetic moments. Near time $t = 0$,

Fig. 4.38: *As an excited magnetic moment relaxes toward its equilibrium position it emits a free induction decay (FID) signal which can be thought of as the transverse component of the precessing moment. In addition, as the moment returns to its equilibrium state the longitudinal component of the magnetic field returns to the value of M_0.*

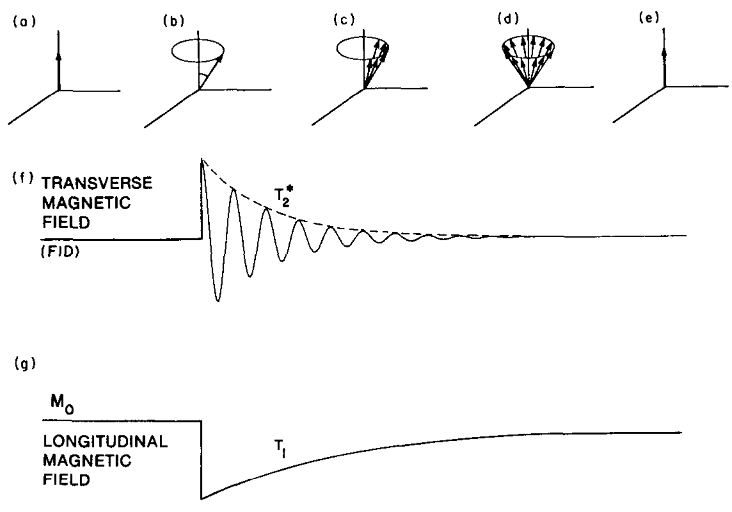

immediately following the end of the RF pulse, the received signal is given by

$$S(t)=\rho \sin(\theta) \cos(\omega_0 t) \tag{63}$$

where again θ is the flip angle and ρ is the density of the magnetic moments. From this signal it is easy to verify that the largest FID signal is generated by a 90° pulse.

Both the spin–spin and the spin–lattice relaxation processes contribute to the decay of the FID signal. The FID signal after a 90° pulse can be written as

$$S(t)=\rho \cos(\omega_0 t) \exp[-t/T_2^*] \exp[-t/T_1] \tag{64}$$

where the exponentials with respect to T_1 and T_2^* represent the attenuation of the FID signal due to the return to equilibrium (T_1) and the dephasing (T_2^*).

In tissue the typical times for T_1 and T_2 are 0.5 s and 50 ms, respectively. Thus the decay of the FID signal is dominated by the spin–spin relaxation time (T_2 and T_2^*) and the effects of the spin–lattice time (e^{-t/T_1} in the equation above) are hidden. A typical FID signal is shown in Fig. 4.38(f).

A clinician is interested in three parameters of the object: spin density, T_1 and T_2. The spin density is easiest to measure; it can be estimated from the magnitude of the FID immediately following the RF pulse. On the other hand, the T_1 and the T_2 parameters are more difficult.

To give our readers just a flavor of the algorithms used in MRI we will only discuss imaging of the spin density. More complicated pulse sequences, such as those described in [Cho82], are used to weight the image by the object's T_1 or T_2 parameters. In addition, much work is being done to discover combinations of the above parameters that make tissue characterization easier.

There are many ways to spatially encode the FID signal so that tomographic images can be formed. We will only discuss two of them here. The first measures line integrals of the object and then uses the Fourier Slice Theorem to reconstruct the object. The second approach measures the two-dimensional Fourier transform of the object directly so that a simple inverse Fourier transform can be used to estimate the object.

To restrict the imaging to a single plane a magnetic gradient

$$\Delta H_p = G_z z \tag{65}$$

is superimposed on the background field H_0 as is shown in Fig. 4.39. If a narrow band excitation at the Larmor frequency $\omega_0 = \gamma H_0$ is then applied to the object only those nuclei near the plane $z = 0$ will be excited. For maximum response the excitation should be long enough to cause each nucleus to precess through 90°.

A projection of the object in the plane $z = 0$ is measured by applying a readout gradient of the form

$$\Delta H_r = G_x x + G_y y \tag{66}$$

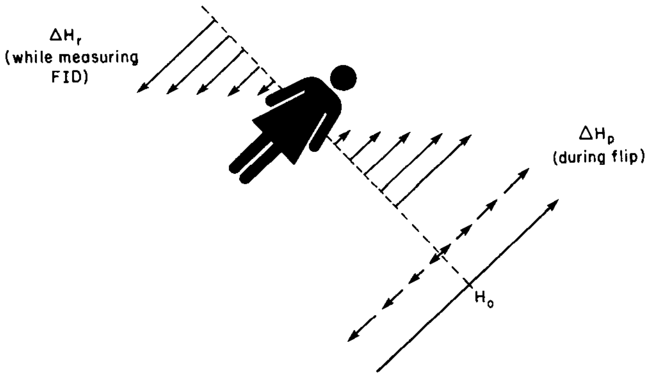

Fig. 4.39: *To measure projections of a three-dimensional object a field of strength $\Delta H_p = G_z z$ used to restrict the initial flip to a single plane. Then a readout gradient $\Delta H_r = G_x x + G_y y$ is used to measure projections of the object. In the case shown here the integrals are along lines perpendicular to the page.*

as the nuclei return to the equilibrium state. This second gradient serves to split each line integral into a separate frequency.

Consider the line

$$G_x x + G_y y = \Delta H_r = \text{constant}. \tag{67}$$

Along this line the FID signal will be at a unique frequency given by

$$\omega = -\gamma(H + \Delta H_r). \tag{68}$$

To measure a projection in the plane it is necessary to apply the readout gradient and then find the Fourier transform of the received signal. Each temporal frequency component of the FID signal will then correspond to a single line integral of the object. This is illustrated in Fig. 4.39.

A two-dimensional reconstruction of an object can be easily found by rotating the readout gradient and then using the reconstruction algorithms discussed in Chapter 3. A full three-dimensional reconstruction is easily formed by stacking the two-dimensional images.

A more common approach to magnetic resonance imaging is to use a phase encoding gradient. The gradient, applied between the excitation pulse and the readout of the FID, spatially encodes each position in the object with a phase. This leads to a very natural reconstruction scheme because data can be collected over a rectangular grid in the Fourier domain. Thus reconstructions using this method can be performed using a two-dimensional FFT instead of the Fourier backprojection usually found in computerized tomography.

One possible sequence of events is presented next. Like the projection approach described above, a magnetic gradient is applied to the object as the nuclei are excited. This restricts the imaging to a single plane where the local magnetic field and the frequency of the excitation satisfy the Larmor equation. This is shown in Fig. 4.40.

Two perpendicular gradients are used to encode each point in the plane. First a gradient, for example in the y direction or $\Delta H_p = G_y y$, is applied for T seconds. Because the frequency of precession is related to the local

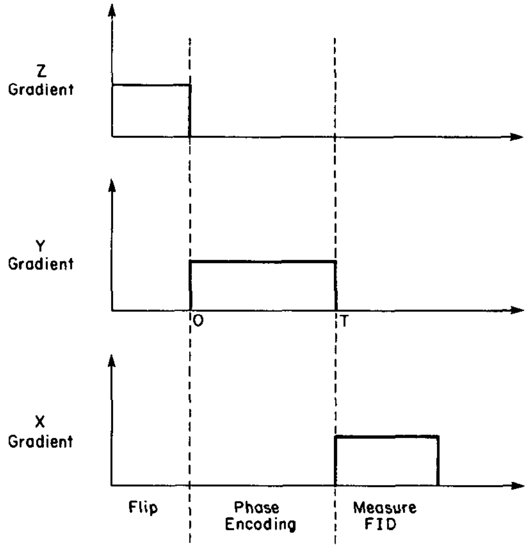

Fig. 4.40: *Three different gradients are used to measure the Fourier transform of an object using MRI. First a gradient in the z direction is used to restrict the flip to a single plane of the object. Then a second gradient, this time in y, is used to encode each line of constant y with a different phase. Finally, a third gradient, in x, is used while the FID signal is read to split each line of constant x into a different line integral.*

magnetic field, nuclei at different points in the object start spinning at different rates. After T seconds, when the phase encoding gradient is turned off, each line of constant y will have accumulated a phase given by

$$\phi = \omega t = (H_0 + \Delta H_p)\gamma T \tag{69}$$

$$= \omega_0 T + G_y y \gamma T. \tag{70}$$

Like the projection case the FID is measured while applying a readout gradient, this time along the x-axis or

$$\Delta H_r = G_x x. \tag{71}$$

As before, the number of spinning nuclei along each line of constant x is now encoded by the frequency of the received signal. Unlike the previous case each position along the line is also encoded with a unique phase (see (69)). The following phase encoded line integral is measured:

$$p_{q_y}(t) = \int\int \rho(x, y) \exp[jyq_y] \exp[jxq_x] \exp[j\omega_0 t] \, dx \, dy \tag{72}$$

where $q_y = G_y \gamma T$ and $q_x = G_x \gamma t$. Note that except for the $e^{j\omega_0 t}$ term this equation is similar to the inverse Fourier transform of the data $\rho(x, y)$. To recover the phase encoded line integrals it is necessary to find the inverse Fourier transform of the data with respect to time or

$$p(w, q_y) = \frac{1}{2\pi} \int p_{q_y}(t) \exp[-jq_x w] \, dq_x. \tag{73}$$

Finally, to recover the phase shifted projections it is necessary to shift the frequency of $p(w, q_y)$ by the Larmor frequency, ω_0, or

$$\rho(x, q_y) = p(w - \omega_0, q_y). \tag{74}$$

A complete reconstruction is formed by stepping the phase encoding gradient, G_y, through N steps between G_{MAX} and $-G_{\text{MAX}}$ and measuring the phase encoded line integrals $p_{q_y}(t)$. To prevent aliasing it is important that

$$G_{\text{MAX}} \gamma T > \frac{\pi}{\Delta} \tag{75}$$

where the minimum feature size in the object is described by Δ. Note that in general the FID signal, $p_{q_y}(t)$, will be sampled in both q_y and t and thus the integral equations presented here will be approximated with discrete summations.

Since each line integral containing the point x, y is encoded with a different phase the spin density at any point can be recovered by inverting the integral equations. This is easily done by finding the Fourier transform of the collection of line integrals or

$$\rho(x, y) = \frac{1}{2\pi} \int p(x, q_y) \exp\left[-jq_y y\right] dq_y. \tag{76}$$

While a reconstruction can be done with either approach most images today are produced by direct Fourier inversion as opposed to the convolution backprojection algorithms described in Chapter 3. Two errors found in MRI machines are nonlinear gradients and a nonuniform static magnetic field. These errors affect the final reconstruction in different ways depending on the reconstruction technique.

First consider nonlinear gradients. In the direct Fourier approach only the magnitude of the gradients changes and not their direction. Thus any nonlinearities show up as a warping of the image space. As long as the gradient is monotonic the image will look sharp, although a bit distorted. On the other hand, in the projection approach the direction of the gradients is constantly changing so that each projection is warped differently. This leads to a blurring of the final reconstruction [ODo85].

The effect is similar with a nonhomogeneous static field, H_0. Since the gradient fields are simply added to the static field to determine the Larmor frequency a nonhomogeneous field can be thought of as a warping of the projection data. Since the Fourier approach doesn't change the angle of the projections, using phase changes to distinguish the different parts of the line integral, the direct Fourier approach yields sharper images.

In the simple analysis above we have ignored two important limitations on MRI. The first is the frequency spreading due to the T_2 relaxation time. In the analysis above we assumed a short enough measurement interval so that the relaxation could be considered negligible. Since the resolution in the frequency domain is linearly dependent on the measurement time the maximum possible measurement time should be used. Unfortunately the exponential attenuation of the FID signal broadens the frequency spectrum thereby determining the ultimate resolution of the magnetic resonance image.

A much more difficult problem is the data collection time. In the procedure described above each measurement is made assuming all the magnetic moments are at rest. Since the spin–lattice relaxation time is on the order of a second this implies that only a single FID can be measured per second. Since a three-dimensional image requires at least a million data points this is a severe restriction.

In practice, pulse sequences have been designed that allow more than one FID to be measured during the T_1 relaxation time. This can be done using a combination of gradients and selective gradients to only excite a single plane within the object and also using selective spin-echo pulses to measure more than one projection (or Fourier transform) within a single plane.

4.5 Bibliographic Notes

Because of the absence of any refraction or diffraction, with x-rays the problem of tomographic imaging reduces to reconstructing an image from its line integrals. A mathematical solution to the problem of reconstructing a function from its projections was given by Radon [Rad17] in 1917. More recently, some of the first investigators to examine this problem either theoretically or experimentally (and often independently) include (in a roughly chronological order): Bracewell [Bra56], Oldendorf [Old61], Cormack [Cor63], [Cor64], Kuhl and Edwards [Kuh63], DeRosier and Klug [DeR68], Tretiak *et al.* [Tre69], Rowley [Row69], Berry and Gibbs [Ber70], Ramachandran and Lakshminarayanan [Ram71], Bender *et al.* [Ben70], and Bates and Peters [Bat71]. A detailed survey of the work done in computed tomographic imaging till 1979 appears in [Kak79].

Detailed information about a number of the applications described in this book is also covered in books by Macovski [Mac83] and Herman [Her80]. For information about alternate approaches to single photon emission tomography the reader is referred to [Kno83]. A more detailed presentation of ultrasound tomography can be found in [Cra82], [Car78b]. Additional information about the physical basis of nuclear magnetic resonance can be found in a number of chemistry and physics texts including [Sha76], [Far71], [Man82], [Pyk82]. The algorithms used to reconstruct images using NMR information are described in [Cho82], [Hin83], [Man82], [Pyk82].

The reader is also referred to [Kak79], [Kak81] for a survey of medical tomographic imaging. For applications in radio astronomy, where the aim is to reconstruct the "brightness" distribution of a celestial source of radio waves from its strip integral measurements taken with special antenna beams, the reader is referred to [Bra56], [Bra67]. For electron microscopy applications, where one attempts to reconstruct the molecular structure of